28th European Young Geotechnical Engineers Conference – EYGEC 2024

A liquefaction simulation for the 1987 Wildlife case study using the extended equivalent linear model (X-ELM)

Samer Abou Kheir[1] , Ziad Kteich[1,2], and Pierre Labbe[2]

[1]*Pole GEOS, TRACTEBEL, Gennevilliers, France*

[2]*ESTP, Cachan, France*

ABSTRACT

Liquefaction-induced ground failure poses significant challenges to engineering practices, particularly in seismic regions. Earthquake events commonly result in liquefaction failures, including settlements, building tilting, sand boils, and slope instabilities. Consequently, assessing liquefaction risk becomes imperative for critical infrastructure. This study introduces a liquefaction simulation approach, specifically tailored for the Wildlife site, utilizing the simplified extended equivalent linear model (X-ELM) method. This method facilitates the simulation of liquefaction within a 1D horizontally layered soil profile. The X-ELM method, being a linear equivalent model, incorporates the effects of pore water pressure buildup through experimental and semi-empirical relationships. It also integrates non-linear soil response due to shear strain and pore water pressure. The practicality of the X-ELM method for engineering applications is emphasized. It is applied to the Wildlife site, which experienced the 1987 Superstition Hills earthquake. The study compares liquefaction triggering response and pore water pressure buildup simulated by the X-ELM method with actual observations from the Wildlife profile array. Through this comparison, the efficacy of the X-ELM method is evaluated, providing insights into its performance and suitability for practical engineering assessments.

KEYWORDS

X-ELM, EERA, Liquefaction, Pore water pressure, Sand, Wildlife site.

1. INTRODUCTION

Probabilistic and statistical analyses of seismic-induced shear stress and experimental soil shear strength have led to the development of empirical methods for assessing liquefaction risk. While simplified methods offer ease of use, they are limited in accuracy and often require significant design margins. In response, complex methods have been proposed to simulate the intricate physics of liquefaction. These methods involve transient nonlinear calculations coupled with excess pore water pressure generation, requiring advanced engineering skills, extensive laboratory tests for soil model calibration, and considerable time investment. As an intermediate solution, the Extended Equivalent Linear Model (X-ELM) offers a simpler approach to studying liquefaction triggers by earthquakes. This method integrates semi-empirical and experimental relationships to combine excess pore water pressure with the linear equivalent response of soil profiles. By doing so, X-ELM provides a more precise and cost-effective means of evaluating liquefaction risk for engineering projects.

In a study by (Kteich, et al., 2019), the X-ELM was applied to twelve soil profiles in the city of Urayasu, where real liquefaction observations were recorded following the 2011 Tohoku earthquake. The X-ELM qualitatively predicted liquefaction occurrences, demonstrating its efficacy. Subsequently, the authors introduced the X-ELM into the VBA/Excel environment for enhanced ease of use in engineering practice. They utilized the model to simulate real observations from the Wildlife profile, comparing the results to in-situ data and acceleration records to assess its reliability. Furthermore, this paper highlights the advantages of utilizing in-situ Cone Penetration Test (CPT) data over Standard Penetration Test

(SPT) data for liquefaction assessment, emphasizing the importance of accurate and comprehensive data inputs in liquefaction risk evaluation.

2. X-ELM/EERA MODEL PRESENTATION

2.1. Theory and background

The extended equivalent linear method X-ELM integrates the excess pore water pressure influence into the conventional equivalent linear method. This method follows the near surface assumption and neglects the effect of volumetric wave propagation. It analyses the response of a 1D soil profile using only the preponderant component of the shear wave with a vertical propagation. To calculate the pore water pressure, this method integrates the generation of the volumetric deformation in function of the shear distortion and the cumulated volumetric deformation using Byrne model (Byrne, 1991). Moreover, it uses the (Martin, et al., 1975) approach and the updated (Wu, 2001) elastic rebound modulus to predict the excess pore water generation into the profile. The previous models combined with an equivalent linear method forms the X-ELM approach, it is used to simulate the response of an undrained soil profile under cyclic loading.

A brief summary of the X-ELM main integrated models will be presented in the following sections, (Kteich, et al., 2019) explain the detailed operation of the X-ELM in his article.

2.2. Modelling of the soil behaviour

The soil response under seismic motion is governed by the shear modulus degradation of the soil profile and is regulated by the intrinsic and geometric energy dissipation of the soil. Based on laboratory tests, it is observed that the soil material under shear loading presents hysteretic response, this behaviour is due to the instantaneous degradation of the shear modulus G in function of the distortion level and the pore water pressure buildup. Equation (1) presents the shear modulus of (Seed & Idriss, 1970) that accounts for the previous observations.

$$G = AF(e)\frac{G}{G_{max}}[\gamma](p')^n \tag{1}$$

AF(e) is considered constant for undrained conditions and can be calculated from the initial maximum shear modulus at very low distortion levels; $\frac{G}{G_{max}}[\gamma]$ is derived from experimental tests on each material, it governs the degradation of the shear modulus in function of the distortion level; $(p')^n$ integrates the influence of the excess pore water pressure on the shear modulus degradation of the soil. (Oztoprak & Bolton, 2013) showed that the experimental shear modulus degradation curves with a maximum of 10 distortion cycles do not incorporate the influence of the pore water pressure. For this reason, the X-ELM incorporate the pore water pressure generation model into the degradation of the soil shear modulus.

2.3. Determination of the volumetric plastic deformation

To determine the pore water pressure generation under undrained cyclic loading, the excess pore water pressure is related to the cumulated volumetric plastic deformation. (Byrne, 1991) proposed equation (2) to quantify the generation of permanent volumetric plastic deformation via cyclic loading. The incremental volumetric deformation is calculated in function of the cumulated deformation, the shear distortion amplitude, and two tuning parameters C1-C2.

$$\Delta\varepsilon_v^p = C_1 exp\left(-C_2\frac{\varepsilon_v^p}{\gamma}\right) \tag{2}$$

Byrne demonstrated that for a single sand with the same relative density a single incremental volumetric deformation curve can be plotted for different distortion level, while a sand with different relative density the fitting curve can be adjusted by updating the volume control C_1 parameter and the shape C_2 parameter. Byrne demonstrated that for different densities the curves preserve identical shapes and proposed relating parameter C_2 to parameter C_1 by the following equation: $C_2 = \frac{0.4}{C_1}$.

The success of the Byrne model derives from the ability to relate : the parameter C_1 with the relative density D_r using equation (3) of (Silver & Seed, 1971) or the normalized SPT blow count $(N_1)_{60}$ using the equation (4) of (Tokimatsu & Seed, 1987) or the corrected equivalent clean sand cone tip resistance q_{c1Ncs} using equation (5) of (Boulanger & Idriss, 2014).

$$C_1 = 7600\ (D_r)^{-2.5} \tag{3}$$

$$C_1 = 8.7\ (N_1)_{60}^{-1.25} \tag{4}$$

$$D_r = \{0.478(q_{C1Ncs})^{0.264} - 1.063\}.100 \tag{5}$$

2.4. Pore water pressure calculation

To determine the excess pore water pressure that is generated from the cumulated plastic volumetric deformation of (Byrne, 1991), the (Martin, et al., 1975) model with the updated (Wu, 2001) rebound modulus is proposed.

The pore water pressure generation is related linearly to the volumetric deformation via the drained bulk modulus. (Seed, et al., 1975) studied the reversibility of the volumetric deformation and noted that it is 20% more reversible in a cyclic loading compared to a monotonic loading. Therefore (Wu, 1996) performed a study to determine the cyclic rebound modulus E_r of the soil and noted that it exists a unique relationship between the soil relative density and the required volumetric deformation to cause liquefaction. Wu proposed the equation (6) to represent the rebound modulus E_r in function of the vertical effective stress and a constant M that is expressed in equation (7) as a function of the SPT $(N_1)_{60}$ and a constant α. The maximum value of M is limited to 480 and the value of α ranges between 150 and 180.

$$E_r = M\sigma'_v \tag{6}$$

$$M = 10(N_1)_{60} + \alpha \tag{7}$$

(Kteich, et al., 2019) proposed equation (8) to calculate the excess pore water pressure considering the corrected rebound modulus of (Wu, 1996) and (Wu, 2001).

$$r_u = \frac{\Delta u}{\sigma'_{v0}} = 1 - exp\ (-M\varepsilon_v^p) \tag{8}$$

To model the response of the soil profile, (Kteich, et al., 2019) integrated the effect of the excess pore pressure into the (Seed, et al., 1975) shear modulus equation as follows:

$$G' = G^0_{max}\frac{G}{G_{max}}[\gamma_{eff}](1 - r_{ueff})^n \tag{9}$$

Integrating the pore water pressure generation model into an equivalent-linear analysis does not consider the instantaneous time effect of the pressure generation and the distortion levels. Therefore, equivalent to the idea proposed by (Seed, et al., 1975) to use an effective distortion level when calculating the shear modulus degradation curve, a weighting coefficient χ is introduced to the pore water pressure ratio $r_{ueff} = \chi r_{umax}$ and integrated into equation (9).

3. CASE STUDY - LIQUEFACTION ANALYSIS OF THE WILDLIFE SITE

3.1. Overview of the Wildlife site

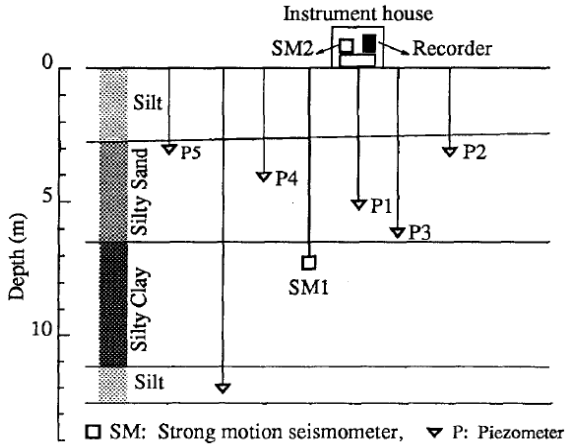

Figure 1. Wildlife profile section and instrumentation. (Bennett, et al., 1984)).

The Wildlife site, situated on the western bank of the Alamo River in Imperial County, Southern California, was flagged for liquefaction susceptibility following observed evidence. To comprehensively understand the interplay between ground motion, pore water pressure buildup, and site degradation, instrumentation was installed to record seismic responses. These data, collected post-liquefaction suspicions, have been pivotal in analyzing the dynamics of ground behavior strength (Bennett, et al., 1984).

The site's profile, illustrated in Figure 1, delineates critical instrumentation placements: the SM2 accelerometer atop the ground surface and the SM1 accelerometer positioned 7.5 meters beneath the silty sand stratum. Identified as liquefiable, the silty sand layer warranted further monitoring, prompting the installation of five piezometers (P1 to P5) to track pore water pressure variations during seismic events. Notably, the water table lies 1.3 meters beneath the ground level, rendering soil layers above this threshold immune to liquefaction.

On November 23, 1987, the Wildlife site experienced the Superstition Hills earthquake, registering a magnitude of Mw=6.6. This seismic event induced a sharp escalation in pore water pressure, as evidenced by field observations revealing the emergence of sand boils—an unmistakable sign of liquefaction occurrence. In response to these findings, the X-ELM approach is proposed to simulate liquefaction dynamics within the Wildlife profile, aiming to enhance understanding and predictive capabilities regarding ground behavior under seismic stressors.

3.2. The X-ELM liquefaction model

The creation of the X-ELM model for the Wildlife site involves utilizing various geotechnical parameters obtained from field investigations and laboratory tests. Figure 2 depicts the SPT N values, shear wave velocity, and Cone Penetration Test (CPT) data, crucial inputs for model development. Additionally, the soil granulometry test conducted by (Bennett, et al., 1984) discerns susceptible zones for liquefaction, utilizing the PS92 criterion for sandy and silty soils and the (Seed et al. 2003) criterion for clayey soils. Regions highlighted in Figures 2 and 3 denote susceptibility to liquefaction.

To refine input parameters for the X-ELM model, the soil fines content is employed to adjust the SPT N values and CPT q_{cN} values, yielding clean sand equivalents $(N_1)_{60CS}$ and $(q_{cN})_{cs}$, respectively. These adjusted values are then incorporated into the (Byrne, 1991) model. Notably, the NS record captured by the SM1 accelerometer, positioned 7.5 meters below the ground surface, is integrated into the X-ELM model with a borehole configuration, accurately simulating motion at this depth layer. This meticulous approach ensures the fidelity of the model in capturing the site-specific dynamics and behavior of the Wildlife site during seismic events.

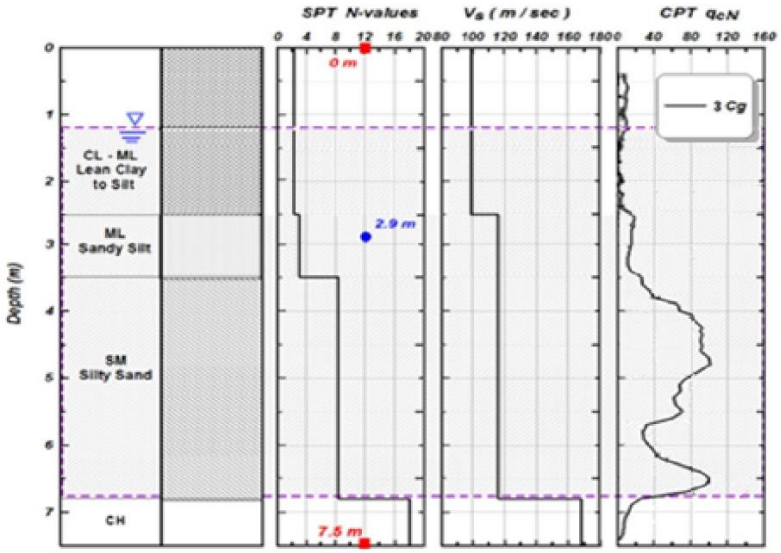

Figure 2. Wildlife liquefaction array profile showing: SPT N values, shear wave velocities, CPT tip resistances, depths of recordings (accelerometers at 0 and 7.5 m; pore-pressure transducer at 2.9 m) and highlighting the liquefiable strata [(Bennett, et al., 1984), (Ziotopoulou, et al., 2012)]

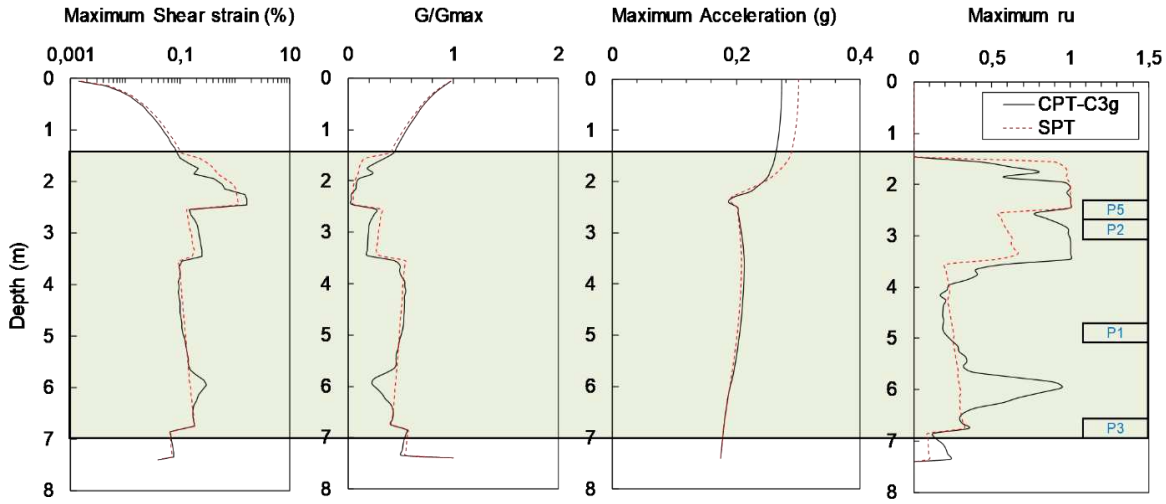

Figure 3. The results of the Wildlife profile showing the maximum shear strain profile, the shear modulus ratio profile, the maximum acceleration profile, the pore water pressure ratio and the highlighted critical layer for the X-ELM model with CPT and SPT input

For comparison, two X-ELM models were developed for the Wildlife profile using in situ data from (Bennett, et al., 1984). These models incorporate adjustments to pore water pressure buildup parameters, namely Byrne C1 and C2, related to the first model with SPT clean sand $(N_1)_{60CS}$ and to the second model with C3g CPT clean sand $(q_{cN})_{cs}$ using using equation (3) and (5). Results from the Wildlife simulation in Figure 3 reveal critical parameters including maximum shear strain, shear modulus ratio, maximum acceleration, and maximum pore water pressure ratio for both X-ELM models. Remarkably, both models exhibit comparable outcomes, with a maximum shear strain of 1.6% and a G/Gmax nearing

0 at a depth of 2.4 meters, indicating a pronounced nonlinear response of the Wildlife profile during the Superstition Hills earthquake.

Applying liquefaction susceptibility criteria, highlighted zones in the Wildlife profile denote regions prone to excess pore water pressure buildup. A notable observation emerges: the model utilizing CPT input presents higher excess pore water pressure ratios, covering a larger area compared to the SPT input model. Furthermore, the SPT input model fails to identify a liquefied zone at a depth of 6 meters. Consequently, the efficacy of liquefaction response assessment hinges on the quality of input profile characteristics, notably observed discrepancies between CPT and SPT inputs. It is evident that the CPT in situ test yields more accurate results, proved more suitable for liquefaction risk assessments.

3.3. Liquefaction results - pore water pressure buildup

Figure 4 presents the pore water pressure buildup visualization, combining in-situ data from piezometers P1, P2, P3, and P5 with the results obtained from the X-ELM model utilizing Cone Penetration Test (CPT) input data. Analysis of the in-situ data reveals a consistent trend in pore water pressure buildup across all four piezometers. This consistency suggests interconnected pores within the susceptible layer, indicating susceptibility to liquefaction across all layers concurrently, typically observed approximately 40 seconds after the onset of shaking. Comparing the pore water pressure buildup between the X-ELM model and real observations, a similar order is noted. Specifically, the pore water pressure buildup (Ru) at P1 and P3 is lower than that at P2 and P5, aligning with the lower soil characteristics observed at P2 and P5 as illustrated in Figure 2. However, while the X-ELM model effectively predicts liquefaction in localized zones, it fails to do so comprehensively. In piezometers P2 and P5, the calculated Ru exceeds the liquefaction triggering threshold of 0.8, indicating liquefaction occurrence. However, despite observed liquefaction, calculated Ru values in piezometers P1 and P3 remain below the triggering limit. Furthermore, the X-ELM model predicts liquefaction occurring after 14 seconds from the onset of the earthquake, contrasting with the 40-second timeframe observed in reality. This discrepancy in timing is attributed to the model's lack of consideration for flow interaction between different layers within the profile. Typically, sand permeability is high, facilitating pressure migration from zones with higher pore water pressure buildup (such as P2 and P5) towards zones with lower buildup (such as P1 and P3), thereby delaying liquefaction occurrence in the former.

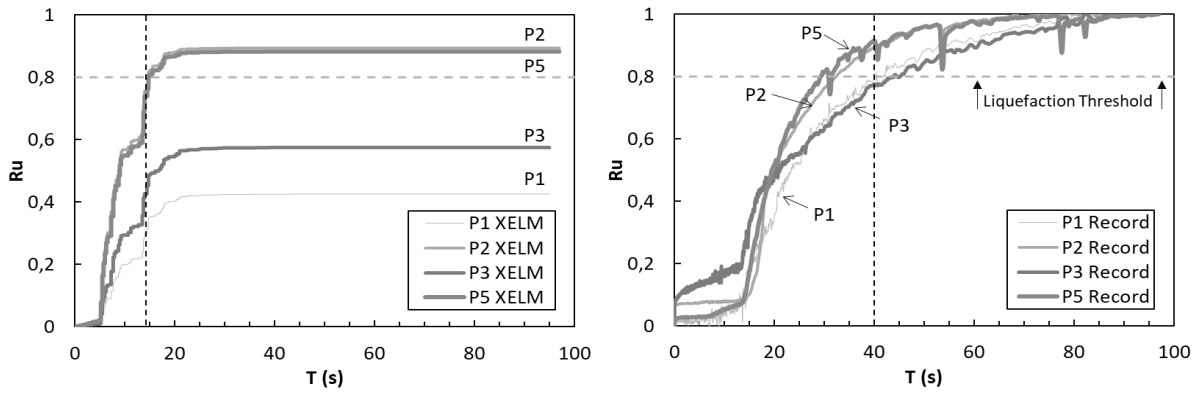

Figure 4. The pore water pressure generation of the X-ELM model for the Wildlife profile and the pore water pressure observations of the P1, P2, P3, and P5 Wildlife

3.4. Liquefaction results - acceleration records

Figure 5 displays the ground surface acceleration records for both the Wildlife real observation and the simulated X-ELM, segmented into four distinct stages for analysis:

- Stage 1 (0.0-13.7 s): During this initial stage, the ground acceleration exhibits a low amplitude (0.13g), accompanied by minimal pore water pressure buildup. The response from the X-ELM simulation closely mirrors the real observation but with smoother amplitude characteristics.

- Stage 2 (13.7-20.6 s): This stage corresponds to the peak of the shaking event, characterized by the strongest ground acceleration reaching a peak of 0.21g. Pore water pressure rapidly increases during this period. While the real observation shows slight smoothing, the X-ELM simulation demonstrates higher peak amplitudes compared to the real observations.
- Stage 3 (20.6-40.0 s): Acceleration amplitudes in the real observation decrease to 0.06g during this stage, accompanied by longer periods compared to previous stages. Pore pressure buildup continues, and the X-ELM simulation exhibits more peaks (higher frequencies) than the recorded data.
- Stage 4 (40.0-96 s): At this stage, excess pore water pressure reaches its maximum value. The registered surface acceleration displays low amplitudes and very high periods, while the X-ELM simulation consistently shows more peaks than the real observations. The smoothing of acceleration amplitudes is attributed to excessive soil softening, where the soil layer undergoes significant deformation and becomes overly plasticized, hindering upward signal transfer.

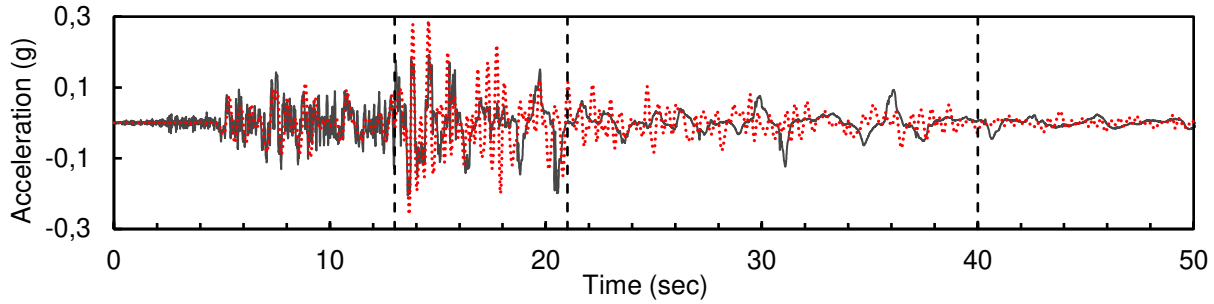

Figure 5. The different stages of the acceleration record at the ground surface level of the Wildlife real observation (solid line) and the simulated X-ELM model (dotted line).

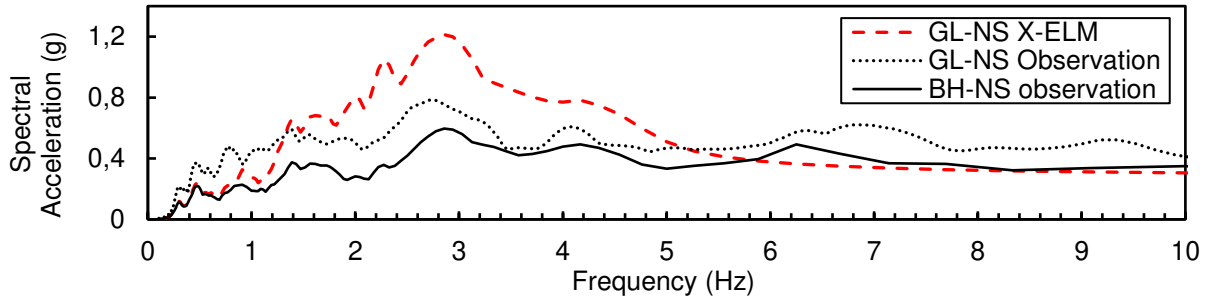

Figure 6. The pseudo spectral acceleration of the Borehole signal for the Wildlife real observation (solid line), the ground surface signal for the Wildlife real observation (soft dotted line), and the ground surface signal for the linear equivalent X-ELM (rough dotted line), with a 5% critical damping ratio.

Figure 6 illustrates the pseudo spectral acceleration of both the real observation and the X-ELM simulation. Notably, all three spectral accelerations exhibit a maximum pseudo spectral acceleration at the same frequency value of 2.9 Hz, indicating that the X-ELM possesses natural frequencies similar to those of the actual profile. However, there are discrepancies in pseudo acceleration amplitudes between the X-ELM model and the real observation. Specifically, the X-ELM model overestimates pseudo acceleration amplitudes within a central frequency range of 1.3 Hz to 5.2 Hz and underestimates them outside this range. The observed decay in high frequencies of the real acceleration record in Figure 5 is attributed to the liquefaction effect. During liquefaction, there is an instantaneous sharp shift in shear modulus and damping values, resulting in a decay of high frequencies in the signal.

The X-ELM model, however, employs a constant and averaged modulus and damping throughout the calculation, incapable of simulating the instantaneous changes in these parameters over time. This averaging effect results in smoothed frequencies in the X-ELM signal, particularly evident in Stage 1. Consequently, the X-ELM model produces lower acceleration amplitudes at high frequency levels.

Conversely, in the low frequency range of the spectrum, the real observation exhibits higher frequencies than the X-ELM simulation in Stages 2, 3, and 4, leading to lower acceleration amplitudes for the X-

ELM. Furthermore, the constant shear modulus over time utilized by the X-ELM model results in amplification at the natural frequencies of the profile, explaining the higher acceleration amplitudes observed at central spectral frequencies.

4. CONCLUSION

The X-ELM method aims to create a liquefaction risk analysis tool that surpasses simple empirical methods in accuracy while maintaining ease of use compared to transient effective stress models. In practice, the X-ELM model successfully identifies soil profile liquefaction triggers during seismic events. However, it diverges from reality in terms of excess pore water pressure generation. Notably, due to the absence of flow calculations, the X-ELM model produces faster pore water pressure changes for highly susceptible layers and slower changes for resistant layers. When assessing liquefaction risk using the X-ELM method, it's crucial to qualitatively consider layer interactions that influence the liquefaction response. In summary, the X-ELM model detects liquefaction but falls short in simulating post-liquefaction effects due to limitations in shear modulus averaging within the linear equivalent method at high distortion and pore water pressure levels.

ACKNOWLEDGEMENT

Sincere gratitude are expressed to TRACTEBEL Engie for funding this work and École des Ponts ParisTech for their academic support during the (GCGOE) master program.

REFERENCES

Bennett, M. J., McLaughlin, P. V., Sarmiento, J. S. & and Youd, T. L., 1984. Geotechnical investigation of liquefaction sites, Imperial Valley, California. *Open-file Rep. 84-252, U.S. Geological Survey, Washington, D.C.*.

Boulanger, R. & Idriss, I., 2014. *CPT and SPT Based Liquefaction Triggering Procedures,* s.l.: Report No. UCD/CGM-14/01, Center for Geotechnical Modeling, University of California, Davis, April 2014.

Byrne, P. M., 1991. *A cyclic shear volume coupling and pore pressure model for sand.* St. Louis, Missouri, USA, s.n.

Kteich, Z. et al., 2019. Extended equivalent linear model (X-ELM) to assess liquefaction triggering: Application to the City of Urayasu during the 2011 Tohuko earthquake. *Soils and Foundations ,* Volume 59(3), 750-763..

Martin, G., Finn, W. & Seed, H., 1975. Fundamentals of liquefaction under cyclic loading. *J. Geotech. Eng. Division, ASCE 101 (GT5),* pp. 423-438.

Oztoprak, S. & Bolton, M., 2013. Stiffness of sands through a laboratory test database. *Geotechnique, 63(1) :54.*

Seed, H. & Idriss, I., 1970. Soil moduli and damping factors for dynamic response analysis. *EERC.*

Seed, H., Idriss, I., Makdisi, F. & Banerjee, N., 1975. Representation of irregular stress times histories by equivalent uniform stress series in liquefaction analyses. *Report No. EERC 75-29.*

Silver, M. & Seed, H., 1971. Deformation characteristics of sands under cyclic loading. *Journal of soil mechanics & foundations Div, 97,* pp. 1081-1098.

Tokimatsu, K. & Seed, H., 1987. Evaluation of settlements in sands due to earthquake shaking. *Journal of geotechnical engineering, 113(8),* pp. 861-878.

Wu, G., 1996. *Volume change and residual pore water pressure of saturated granular soils to blast loads.,* Burnaby: The natural sciences and engineering research council of canada AGRA earth & Environmental Ltd.,.

Wu, G., 2001. earthquake-induced deformation analyses of the upper san fernando dam under the 1971 san fernando earthquake. *Canadian geotechnical journal, 38(1) : 1-15.*

Ziotopoulou, k., Boulanger, R. W. & Kramer, S. L., 2012. *Site Response Analysis of Liquefying Sites.* , s.n.